Multiscale methods for two and three-phase flow simulation in subsurface petroleum reservoirs

Mayur Pal* Sadok Lamine* Knut-Andreas Lie† Stein Krogstad†

September 13, 2012

Abstract

Subsurface reservoirs generally have a complex description in terms of both geometry and geology. This poses a continuing challenge in modelling and simulation of reservoirs due to variations at different length scales. Multiscale simulation is a new and promising approach that enables simulation of detailed geological model and the retention of level of detail and heterogeneity that would not be possible via conventional upscaling methods. Most multiscale methods are developed from a sequential formulation, in which flow (pressure-flux) and transport (saturation) equations are solved in separate steps. The flow equation is solved using a set of special multiscale basis functions that attempt to incorporate the effects of sub-grid geological heterogeneity into a global flow equation formulated on a coarsened grid. The multiscale basis functions are computed numerically by solving local flow problems, and can be used to construct conservative fluxes on the coarsened as well as the original fine grid.

Herein, we consider one particular multiscale method, the multiscale mixed finite-element method, and discuss how it can be extended to account for capillary pressure effects. The method is evaluated for computational efficiency and accuracy on a series of models with a high degree of realism, including spatially dependent relative permeability and capillary effects, gravity, and highly heterogeneous rock properties specified on representative corner-point grids.

*Shell Global Solutions International B.V. Kessler Park 1, 2288 GS, Rijswijk, The Netherlands.
Email: mayur.pal@shell.com, sadok.lamine@shell.com

†SINTEF ICT, Department of Applied Mathematics P.O. Box 124 Blindern, N-0314 Oslo, Norway
Email: Knut-Andreas.Lie@sintef.no, Stein.Krogstad@sintef.no

Introduction

A major challenges in modeling petroleum recovery processes is that the flow of hydrocarbons is affected by physical processes occurring on multiple length (and time) scales. Whereas a hydrocarbon reservoir is usually of the scale of miles in the areal dimensions, the reservoir properties (e.g., porosity and permeability) typically show strong heterogeneity and may vary over many scales from the pore scale (10 μm), via the core scale (10 cm), to the geological scale (1 km). Modern reservoir characterization and geostatistical modeling techniques are able to integrate information from these different scales to build geo-cellular models that describe the reservoir properties in great details, having the order of 10^7–10^9 grid cells. Unfortunately, it is too expensive to solve multi-phase flow problems on such high-resolution models, even with modern day computer power; typically, a reservoir simulator handles simulation models with 10^5–10^7 grid cells. The standard approach is therefore to perform simulations using coarse-scale simulation models that are usually created by employing some sort of upscaling work-flow, thereby losing potentially important fine-scale properties.

In the past few years, there has been an increasing interest in methods that are designed to accurately and effectively solve problems having multiple scales. The so-called multiscale methods combine fine and coarse-scale computations to resolve the most important fine-scale information efficiently on a coarser scale without having to compute directly on the global fine-scale problem. For reservoir simulation, this means that fine-scale petrophysical and geological details are captured directly into the coarse-scale simulation model.

Several multiscale methods [11] applicable to petroleum reservoir simulation have been presented in the literature, including dual-grid methods [5–7, 13], (adaptive) local-global methods [9, 10], finite-element methods [16], mixed finite-element methods [1–4, 8], and finite-volume multiscale methods [14, 15, 17, 23]. The methods are algorithmically different, but share the same basic concept of incorporating fine-scale information into coarse-scale equations via some sort of numerically constructed functions. These functions, also known as basis functions, contain fine-scale information embedded in the solution and are coupled through a global formulation to provide an accurate approximation of the flow solution. In a typical multiscale method, the pressure is first computed on a coarse grid, after which the solution is propagated to a finer grid using the basis functions. These basis functions can be computed locally, globally, or by using an adaptive local-global approach [4] to set boundary conditions that are required to subsequently compute the saturation change on the finer grid. In this two-grid approach, the pressure and saturation equations are decoupled. The pressure equation is solved on a coarse grid from which a mass-conservative fine-scale velocity field is recovered and used to solve the transport equation on the underlying fine grid.

Multiscale methods should not be confused with upscaling; there are some similarities but also significant differences. A comprehensive comparison of multiscale method with state-of-the-art upscaling methods for elliptic problems in porous media is presented by Kippe et al. [18]. The main objective of the multiscale method is to obtain efficient and accurate approximations on a fine or intermediate scale, whereas the intent of upscaling is to generate approximate coarse-scale solutions [12]. Moreover, the natural coupling between local and global scales in multiscale methods avoids the inconsistency and non-physical coarse-scale properties that are often associated with many upscaling techniques.

In this paper, we present a multiscale mixed finite-element (MsMFE) method that accounts for gravity, relative permeability and capillarity. The MsMFE is applied to simulate two-phase incompressible flow on challenging geologically realistic corner-point grids and benchmarked against an industry-standard fine-scale solver. In addition, we present some preliminary results from application of the method to compressible 3-phase flow, see [19, 20] for more details. The multiscale formulations presented in this paper have been implemented in the MATLAB Reservoir Simulation Toolbox (MRST) [24, 27] and all numerical results presented are generated by using this toolbox.

Mathematical model

The partial differential equations governing two-phase incompressible flow in a porous medium can be derived from (i) the continuity equation over each phase α

$$\frac{\partial(\rho_\alpha S_\alpha \phi)}{\partial t} + \nabla \cdot (\rho_\alpha \vec{v}_\alpha) = q_\alpha, \tag{1}$$

over an arbitrary domain Ω, and (ii) Darcy's law describing relationship between phase velocity $\vec{v}_\alpha$ and phase pressure p_α:

$$\vec{v}_\alpha = -\mathbf{K}\lambda_\alpha(\nabla p_\alpha - g\rho_\alpha \nabla z). \tag{2}$$

In Eq. (1), the phase saturation S_α represents the fraction of accessible pore volume filled by a phase α, ρ_α is the density of phase α, and q_α denotes the sources/sink terms representative of well injection/production rates. We assume that the two phases, water (w) and oil (o), fill the pore volume, $S_o + S_w = 1$. The permeability tensor $\mathbf{K}$ is either diagonal or full and will typically be discontinuous across internal boundaries of the domain Ω. Moreover, ϕ denotes the porosity and $\lambda_\alpha = k_{ri}/\mu_\alpha$ the phase mobility, in which k_{ri} and μ_α denote the relative permeability and viscosity of phase α, respectively.

To better reveal the nature of the mathematical model, it is common to reformulate (1)–(2) as a flow equation for fluid pressure and a transport equation for saturation. We assume that the fluids are immiscible and incompressible. We then define the total flow rate $q = q_o + q_w$ and introduce the total mobility $\lambda = \lambda_w + \lambda_o$, the fractional flow function $f_\alpha = \lambda_\alpha/\lambda$, the total velocity $\vec{v} = \vec{v}_w + \vec{v}_o$, and the capillary pressure $p_c = p_o - p_w$. Darcy's law in combination with conservation of mass results in the pressure equation that can be used to solve for the total velocity

$$\nabla \cdot \vec{v} = q, \qquad \vec{v} = -\mathbf{K}\lambda\left[\nabla p_o - \tilde{g}(S_w)\nabla z + h(S_w)\nabla p_c\right], \tag{3}$$

where $\tilde{g}(S_w) = (f_w(S_w)\rho_w + f_o(S_w)\rho_o)g$. The form of the function $h(S_w)$ depends upon the choice of primary pressure variable. Here, we will use oil pressure, for which $h(S_w) = f_w(S_w)$. Finally, we use Eq. (1) to derive the saturation equation (transport equation for the water phase)

$$\phi\frac{\partial S_w}{\partial t} + \nabla \cdot f_w(S_w)\left[\vec{v} + \mathbf{K}\lambda_o(S_w)\left((\rho_w - \rho_o)g\nabla z + \nabla p_c(S_w)\right)\right] = \frac{q_w}{\rho_w}. \tag{4}$$

For simplicity, we will henceforth drop the subscripts on the primary variables p and S.

Fine-scale discretization

Consider the partitioned computational domain Ω into a set $\{C_i\}$ of N non-overlapping polyhedral cells, where each cell i can have a varying number of n_i planar faces that match the faces of the cell's neighbours. To solve the system (3)–(4), we will use a sequential procedure in which we first compute the solution of the elliptic pressure equation (3) to provide explicit fluxes at the cell interfaces, which subsequently are used to evolve the parabolic transport equation (4).

Pressure equation

Let u_i be the vector of outward fluxes from cell C_i, let p_i denote the pressure at the cell centre and π_i the pressure at the cell faces. Discretization methods used for reservoir simulation are constructed to be locally conservative and exact for linear solutions. Such schemes can be written in a form that uses Darcy's law to relate the three quantities $\mathbf{u}$, p, and π through a matrix $\mathbf{T}_i$ of one-sided transmissibilities,

$$\mathbf{u}_i = \mathbf{T}_i\left[\mathbf{e}_i p_i - \pi_i - \tilde{g}(S_i)\Delta\mathbf{z}_i + h(S_i)\left(\mathbf{e}_i p_c(\vec{x}_i, S_i) - \mathbf{p}_{ci}\right)\right], \quad \mathbf{e}_i = (1,...,1)^T. \tag{5}$$

Here, $\Delta\mathbf{z}_i$ denotes the vector of differences in the z-coordinate of the cell centre $\vec{x}_i$ and the face centroids. Moreover, we have defined the capillary pressure $\mathbf{p}_{ci}$ at the cell faces as the linear interpolation of the

capillary pressure in the neighbouring cells. The one-sided transmissibilities $\mathbf{T}_i$ are associated with pressure difference between cells centres and pressure continuity points on cell faces, other methods for computing transmissibilities using multi-point fluxes, commonly known as MPFA, may also be used, see [25, 26, 28] for details and references therein. Augmenting (5) with flux and pressure continuity across cell faces, we get the following linear system

$$\begin{bmatrix} \mathbf{B} & \mathbf{C} & \mathbf{D} \\ \mathbf{C}^{\mathsf{T}} & \mathbf{0} & \mathbf{0} \\ \mathbf{D}^{\mathsf{T}} & \mathbf{0} & \mathbf{0} \end{bmatrix} \begin{bmatrix} \mathbf{u} \\ -\mathbf{p} \\ \pi \end{bmatrix} = \begin{bmatrix} -\mathbf{G}(\mathbf{S})\Delta\mathbf{z} + \mathbf{H}(\mathbf{S})\Delta\mathbf{p}_c \\ \mathbf{q} \\ \mathbf{0} \end{bmatrix}, \tag{6}$$

where the first row in the block-matrix equation (6) corresponds to Equation (5) for all grid cells. Thus, $\mathbf{u}$ denotes the outward face fluxes ordered cell wise (fluxes over interior faces and faults appear twice with opposite signs), $\mathbf{p}$ denotes the cell pressure, and π the face pressures, where each side in presence of a fault is considered as separate face. The right hand terms $\mathbf{G}(\mathbf{S})\Delta\mathbf{z}$ and $\mathbf{H}(\mathbf{S})\Delta\mathbf{p}_c$ are the one-sided face contributions corresponding to gravity and capillary effects, respectively, as defined in (5). The matrices $\mathbf{B}$ and $\mathbf{C}$ are block diagonal with each block corresponding to a cell. For the two matrices, the i^{th} blocks are given as $\mathbf{T}_i^{-1}$ and $\mathbf{e}_i$, respectively. Similarly, each column of $\mathbf{D}$ corresponds to a unique face and has one (for boundary faces) or two (for interior faces) unit entries corresponding to the index of the face in the cell wise ordering.

Transport equation

The transport equation (4) will be solved on the fine-scale grid consisting of cells C_i, assuming that we have a set of mass-conservative fluxes $\mathbf{u}$. To compute the contributions from the ∇p_c on a face between two neighbouring cells i, j, we use a two-point difference

$$\mathbf{K}\nabla p_c(S) \approx \mathbf{K}_h\big(p_c(S_i) - p_c(S_j)\big)/|\vec{c}_{ij}|, \tag{7}$$

where $\vec{c}_{ij}$ is the centroid difference between cells i and j and $\mathbf{K}_h$ denotes the harmonic average of the cell permeabilities in the direction of the face normal. Using a standard single-point upstream weighting method, the saturation equation can then be discretized as follows (with a slight abuse of notation):

$$S^{n+1} = S^n - \frac{\Delta t}{\Phi}([\mathbf{U} + \Lambda_o(S^m)(\hat{\mathbf{G}}\Delta\mathbf{z} + \mathbf{P}_c(S^m))]\mathbf{F}_w(S^m) - \max(\mathbf{q},0) - \mathbf{f}_w(S^m)\min(\mathbf{q},0). \tag{8}$$

Here, Φ is a diagonal matrix of pore volume, while $\mathbf{U}$, $\hat{\mathbf{G}}$, and $\mathbf{P}_c$ are matrices (with dimension equal the number of cells times the number of faces) giving the flux contribution from Darcy fluxes, gravity, and capillary pressure for each face. The diagonal matrix Λ_o and the vector $\mathbf{f}_w$ denote the upstream weighted oil mobility and fractional flow, respectively. The discretization may be explicit ($m = n$) or implicit ($m = n+1$) and the numerical accuracy can (of course) be improved by using higher-order upwind schemes, like the wave-oriented multi-dimensional schemes [21, 22].

The multiscale mixed finite-element (MsMFE) method

The multiscale method is formulated based on two hierarchically nested grids, Figure 1, a fine-scale grid on which the rock and rock-fluid properties are given and a coarse simulation grid to which we associate the degree-of-freedom used to solve the global flow problem. Each block of the coarse grid consists of a connected set of cells from the fine grid. In principle, the blocks can have almost arbitrary shapes as long as they are singly connected. However, the best numerical resolution is obtained if their shapes are somewhat regular and adapt to distinct geological features [3]. The key idea of the multiscale mixed method is to construct a special approximation space, consisting of a set of coarse-scale basis functions that solve the flow equation locally. The local flow problems will be driven by source terms rather than boundary conditions, which are normally used in flow-based upscaling. Using these local basis functions, the effects of the fine-scale heterogeneity can be incorporated into the discretized coarse-scale flow problem in a way that is consistent with the local fine-scale properties of the differential operators. Figure 1 summarises our workflow for multiscale simulation.

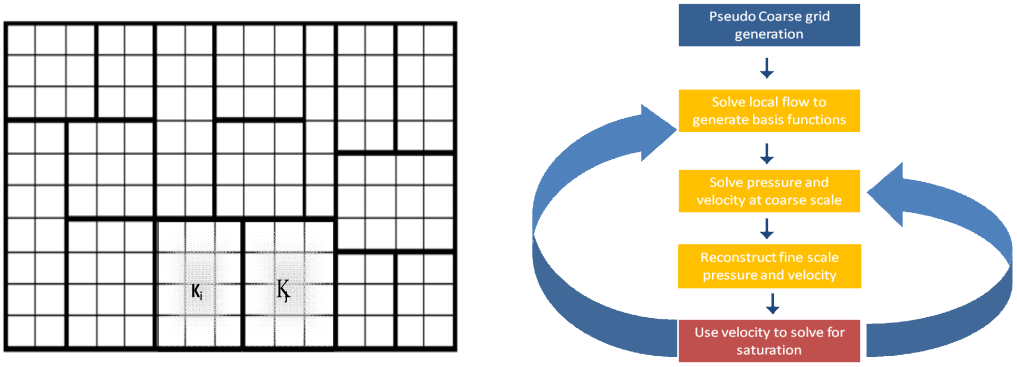

Figure 1 *The left plot shows the coarse grid for MsMFE defined hierarchically on top the fine grid so that each coarse block consists of a singly-connected set of cells. The diagram to the right shows the workflow for multiscale simulation using the MsMFE method.*

Multiscale approximation. To formally define the MsMFE method, we start by decomposing the solution to (6) as follows

$$\mathbf{u} = \Psi \mathbf{u}_c + \tilde{\mathbf{u}}, \qquad \mathbf{p} = \Phi \mathbf{p}_c + \tilde{\mathbf{p}}, \qquad \pi = \Pi \pi_c + \tilde{\pi}. \tag{9}$$

Here, $\mathbf{u}_c$ denotes the vector of outward fluxes over the coarse-block interfaces, $\mathbf{p}_c$ denotes the vector of coarse-block pressures, and π denotes the vector of coarse-block face pressures. Likewise, $\tilde{\mathbf{u}}$, $\tilde{\mathbf{p}}$, $\tilde{\pi}$ are reminder terms having variations on the fine grid. The matrices Ψ, Φ, and Π represent the fine-scale reconstruction operators for $\vec{v}$, p, and π. Each column in Ψ corresponds to a multiscale basis function for the flux associated with a unique coarse-grid face and is represented as a $n_f \times 1$ vector of fine-scale fluxes.

For compressible flow, we also need to define fine-scale variations for the pressure basis so that each column of Φ corresponds to a basis function associated with unique cell and each column of Π corresponds to a basis function defined over a coarse face. For incompressible flow, on the other hand, pressure is seldom used explicitly except to determine well-rates through the use of appropriate well models and we therefore define the pressure to be constant within each coarse block. This means that Φ can be replaced by a simple prolongation operator $\mathbf{I}$ that maps a constant value from each coarse block and onto the cells of the block. Likewise, Π is replaced by a prolongation operator $\mathbf{J}$ that maps a constant value from each coarse face and onto the cell faces that make up the coarse face. Hence, we have now defined a reconstruction operator $\mathbf{R} = \mathrm{diag}(\Psi, \mathbf{I}, \mathbf{J})$ that brings us from the degrees-of-freedom $\mathbf{x}_c = [\mathbf{u}_c, -\mathbf{p}_c, \pi_c]$ on the coarse-scale to those on the fine scale $\mathbf{x} = [\mathbf{u}, -\mathbf{p}, \pi]$.

Coarse system. To form a global system on the coarse grid, we first notice that the transposed of the prolongation operators $\mathbf{I}$ and $\mathbf{J}$ correspond to the sum over all fine cells of a coarse block and all fine-cell faces that are part of the faces of the coarse blocks, respectively. It is therefore natural to choose $\mathbf{R}^\mathsf{T}$ as our compression operator. We then multiply (6) from the left by $\mathbf{R}^\mathsf{T}$, substitute $\mathbf{x} = \mathbf{R}\mathbf{x}_c$, and rearrange terms to obtain the following coarse-scale system

$$\begin{bmatrix} \Psi^\mathsf{T}\mathbf{B}\Psi & \Psi^\mathsf{T}\mathbf{C}\mathbf{I} & \Psi^\mathsf{T}\mathbf{D}\mathbf{J} \\ \mathbf{I}^\mathsf{T}\mathbf{C}^\mathsf{T}\Psi & \mathbf{0} & \mathbf{0} \\ \mathbf{J}^\mathsf{T}\mathbf{D}^\mathsf{T}\Psi & \mathbf{0} & \mathbf{0} \end{bmatrix} \begin{bmatrix} \mathbf{u}_c \\ -\mathbf{p}_c \\ \pi_c \end{bmatrix} = \begin{bmatrix} \Psi^\mathsf{T}\left(\mathbf{H}(\mathbf{S})\Delta\mathbf{p}_c - \mathbf{G}(\mathbf{S})\Delta\mathbf{z}\right) - \Psi^\mathsf{T}\left(\mathbf{B}\tilde{\mathbf{u}} - \mathbf{C}\tilde{\mathbf{p}} + \mathbf{D}\tilde{\pi}\right) \\ \mathbf{I}^\mathsf{T}\mathbf{q} - \mathbf{I}^\mathsf{T}\mathbf{C}^\mathsf{T}\tilde{\mathbf{u}} \\ -\mathbf{J}^\mathsf{T}\mathbf{D}^\mathsf{T}\tilde{\pi} \end{bmatrix}. \tag{10}$$

Next, we need to make certain modelling assumptions to eliminate the fine-scale reminder terms. First, we observe that if Ψ is obtained by solving local problems, Darcy's law says that each column of Ψ must satisfy an equation of the form $\mathbf{C}^\mathsf{T}\Psi_i = \mathbf{w}$, where $\mathbf{w}$ is a vector of source terms used to drive the flow modelled by the basis function. In an incompressible flow model the pressure is immaterial,therefore,

we can pick $\tilde{\mathbf{p}}$ such that $\mathbf{w}^{\mathsf{T}}\tilde{\mathbf{p}} = 0$ for each block. This defines a unique splitting $\mathbf{I}\mathbf{p}_c + \tilde{\mathbf{p}}$ and implies that the coarse-scale pressure is the w-weighted average of the true pressure, $p_c^i = \int_{B_i} w p \, d\vec{x}$. By neglecting the contributions from the other two remainder terms $\tilde{\mathbf{u}}$ and $\tilde{\pi}$, we end up with the coarse-scale system

$$\begin{bmatrix} \Psi^{\mathsf{T}}\mathbf{B}\Psi & \Psi^{\mathsf{T}}\mathbf{C}\mathbf{I} & \Psi^{\mathsf{T}}\mathbf{D}\mathbf{J} \\ \mathbf{I}^{\mathsf{T}}\mathbf{C}^{\mathsf{T}}\Psi & \mathbf{0} & \mathbf{0} \\ \mathbf{J}^{\mathsf{T}}\mathbf{D}^{\mathsf{T}}\Psi & \mathbf{0} & \mathbf{0} \end{bmatrix} \begin{bmatrix} \mathbf{u}_c \\ -\mathbf{p}_c \\ \pi_c \end{bmatrix} = \begin{bmatrix} \Psi^{\mathsf{T}}\big(\mathbf{H}(\mathbf{S})\Delta\mathbf{p}_c - \mathbf{G}(\mathbf{S})\Delta\mathbf{z}\big) \\ \mathbf{I}^{\mathsf{T}}\mathbf{q} \\ \mathbf{0} \end{bmatrix}. \tag{11}$$

Multiscale basis functions. Herein, we will use the so-called two-block method to compute basis functions which does not impose any condition on the coarse interface to which the basis function is associated. Although the two-block method is not convergent, it will typically give good accuracy on finite grids. In the alternative single-block method, one has to specify fine-scale fluxes over the interface and this method is only accurate when using fluxes that carry global flow information. Consider two neighbouring blocks B_i and B_j, and let B_{ij} be a singly-connected subset of Ω that contains B_i and B_j. If we neglect the influence of gravity and capillary forces, a multiscale basis function associated with the interface $\Gamma_{ij} = \partial B_i \cap \partial B_j$ can the be computed by solving

$$\vec{\psi}_{ij} = -\mathbf{K}\nabla\phi_{ij}, \qquad \nabla\cdot\vec{\psi}_{ij} = w_{ij}(\vec{x}) = \begin{cases} w_i(\vec{x}), & \text{if } \vec{x}\in B_i, \\ -w_j(\vec{x}), & \text{if } \vec{x}\in B_j, \\ 0, & \text{otherwise}, \end{cases} \tag{12}$$

in B_{ij} with $\vec{\psi}_{ij}\cdot\vec{n} = 0$ on ∂B_{ij}. If $B_{ij} \neq B_i \cup B_j$, we say that the basis function is computed using *overlap* or *oversampling* to lessen the impact of the artificial no-flow condition on the boundary.

The purpose of the weight function $w_{ij}(\vec{x})$ is to distribute the divergence of the velocity, $\nabla\cdot\vec{v}$ over the coarse block and produce a flow with unit flux over the interface Γ_{ij}. To produce a unit flow across the interface Γ_{ij}, the weight function should be chosen on the form $w_i(\mathbf{x}) = \theta(\mathbf{x})/\int_{B_i}\theta(\mathbf{x})d\mathbf{x}$. The function $\theta(x)$ can be defined in several ways. Solving for the flux field using an incompressible flow model, a natural choice would be to use Raviart–Thomas mixed finite-element method on the coarse scale for rectangular blocks. This means, to solve the local sub problems such that they reconstruct the Raviart–Thomas basis functions on the coarse scale. For this choice, it is common to use $\theta(\vec{x}) \equiv 1$ or $\theta(\vec{x}) = \text{trace}(\mathbf{K})$ away from the possible wells and $\theta(\vec{x}) = q(\vec{x})$ in grid blocks penetrated by wells; for more details, please see [1–4, 17].

Accounting for capillary forces. In principle, fine-scale flow effects from capillary pressure could be accounted for using basis functions defined from the following equation

$$\vec{\psi}_{ij} = -\mathbf{K}\big(\nabla\phi_{ij} - h(S)\nabla p_c(S)\big), \qquad \nabla\cdot\vec{\psi}_{ij} = w_{ij}(\vec{x}). \tag{13}$$

There are two main drawbacks with this approach. First of all, since the basis functions are solved as reference problems that do not consider the actual physical magnitude of the flux, it will be a challenge to obtain the correct scaling of the contributions from the capillary pressure compared relative to the source term. Secondly, because the capillary pressure function is saturation dependent, the basis functions will be strongly time dependent and will need to be updated regularly. To avoid the first problem (and reduce the second), we will instead use two sets of basis functions: one without capillary pressure computed from (12) and a separate basis for capillary pressure computed from

$$\vec{\psi}^c_{ij} = -\mathbf{K}\big(\nabla\phi^c_{ij} - h(S)\nabla p_c(S)\big), \qquad \nabla\cdot\vec{\psi}^c_{ij} = 0. \tag{14}$$

Extension to compressible flow. Finally, we briefly review how the multiscale method can be extended to compressible flow. Consider a model written on the compact form

$$\nabla\cdot\vec{v} = q - c_t\frac{\partial p}{\partial t} + \Big(\sum_j c_j f_j\vec{v} + \alpha(p)\mathbf{K}\vec{g}\Big)\cdot\nabla p, \quad \vec{v} = -\lambda\mathbf{K}\big(\nabla p - \sum_j \rho_j f_j\vec{g}\big). \tag{15}$$

Here, ρ_j denotes phase densities, f_j fractional flow functions, $\vec{g}$ the gravity vector, c_j and c_t the phase and total compressibilities, and $\alpha(p)$ a known function of pressure-dependent parameters. Linearizing (15) a mimetic discretization $\mathbf{v}_i = \mathbf{T}_i(p_i\mathbf{e}_i - \pi_i)$, we derive a mixed discrete system of the form

$$\begin{bmatrix}\mathbf{B}^n & \mathbf{C}\\ \mathbf{C}^\mathsf{T} & \mathbf{P}^n(\mathbf{p}_{\nu+1}^{n+1})\end{bmatrix}\begin{bmatrix}\mathbf{v}_{\nu+1}^{n+1}\\ -\mathbf{p}_{\nu+1}^{n+1}\end{bmatrix} = \begin{bmatrix}\mathbf{f}^n(\mathbf{p}_\nu^{n+1})\\ \mathbf{g}^n(\mathbf{p}^n,\mathbf{p}_\nu^{n+1})\end{bmatrix}. \tag{16}$$

Here, n denotes time steps and ν iteration steps. The superscript n indicates that the matrices $\mathbf{B}$ and $\mathbf{P}$ and the vectors $\mathbf{f}$ and $\mathbf{g}$ are functions of the saturation at time step n and will henceforth be dropped for brevity. For compressible flow, the pressure is no longer immaterial and we therefore have to include subscale variation also for the pressure. Discretizing the elliptic basis functions, we observe that

$$\mathbf{B}\Psi - \mathbf{C}\Phi = \mathbf{0} \quad\Longrightarrow\quad \mathbf{B}\Psi\mathbf{v}_c - \mathbf{C}\Phi\mathbf{v}_c = \mathbf{0},$$

which implies that Φ and Ψ should scale similarly. For the pressure we will therefore use a multiscale decomposition of the form $\mathbf{p} = \mathbf{I}\mathbf{p}_c + \Lambda\Phi\mathbf{v}_c + \tilde{\mathbf{p}}$, where $\Lambda = \mathrm{diag}(\lambda_i^0/\lambda_i)$ accounts for saturation variations. Introducing the compression operator $\mathrm{diag}(\Psi^\mathsf{T},\mathbf{I}^\mathsf{T})$ and neglecting residual terms, we obtain the coarse-scale compressible system

$$\begin{bmatrix}\Psi^\mathsf{T}\mathbf{B}\Psi & \Psi^\mathsf{T}\mathbf{C}\mathbf{I}\\ \mathbf{I}^\mathsf{T}(\mathbf{C}^\mathsf{T}\Psi - \mathbf{P}_\nu\Lambda\Phi) & \mathbf{I}^\mathsf{T}\mathbf{P}_\nu\mathbf{I}\end{bmatrix}\begin{bmatrix}\mathbf{v}_c^{\nu+1}\\ -\mathbf{p}_c^{\nu+1}\end{bmatrix} = \begin{bmatrix}\Psi^\mathsf{T}\mathbf{f}_\nu\\ \mathbf{I}^\mathsf{T}\mathbf{g}_\nu\end{bmatrix}. \tag{17}$$

To get an approximation that converges to the solution of the fine-scale discrete equation, we also include an equation for the residual terms

$$\begin{bmatrix}\mathbf{B} & \mathbf{C}\\ \mathbf{C}^\mathsf{T} & \mathbf{P}\end{bmatrix}\begin{bmatrix}\hat{\mathbf{v}}^{\nu+1}\\ -\hat{\mathbf{p}}^{\nu+1}\end{bmatrix} = \begin{bmatrix}\mathbf{f}_c - \Psi^\mathsf{T}\mathbf{B}\Psi\mathbf{v}_c + \Psi^\mathsf{T}\mathbf{C}\mathbf{I}\mathbf{p}_c\\ \mathbf{g}_c - \mathbf{I}^\mathsf{T}(\mathbf{C}^\mathsf{T}\Psi - \mathbf{P}_\nu\Lambda\Phi)\mathbf{v}_c + \mathbf{I}^\mathsf{T}\mathbf{P}_\nu\mathbf{I}\mathbf{p}_c\end{bmatrix}, \tag{18}$$

which we will solve using a standard overlapping Schwarz method. The resulting iterative method, iMsMFE for short, consists of an outer loop in which we iterate over (17) and (18) to reduce the fine-scale residual, and an inner loop that is used to solve each of the equations (17) and (18).

Numerical results

In this section, we will evaluate the MsMFE method on test cases involving realistic reservoir geometries and properties. The first two cases aim to validate the multiscale method for incompressible two-phase flow with gravity and spatially dependent capillary pressure and relative permeability. The first test case involves two regions with different relative permeability and capillary curves. The second test corresponds to a sector model with multiple regions with a different relative permeability and capillary curve associated with each region. The third case demonstrates the use of MsMFE for compressible three phase flow.

Example 1 (Box geometry with two saturation regions) *This test case consists of a simple box-type geometry with two saturation regions with homogeneous porosity and permeability, but different relative permeability and capillary curves, see Figure 2. The fine grid has* $20\times20\times1$ *cells, which we have partitioned uniformly into* $5\times5\times1$ *coarse blocks. Permeability of the medium is 100mD and porosity is 0.3. An injector and a producer are located in the middle of the bottom and top part of the reservoir, respectively. The reservoir is initially fully saturated with oil. Water is injected at the rate of 0.5* m^3*/day*

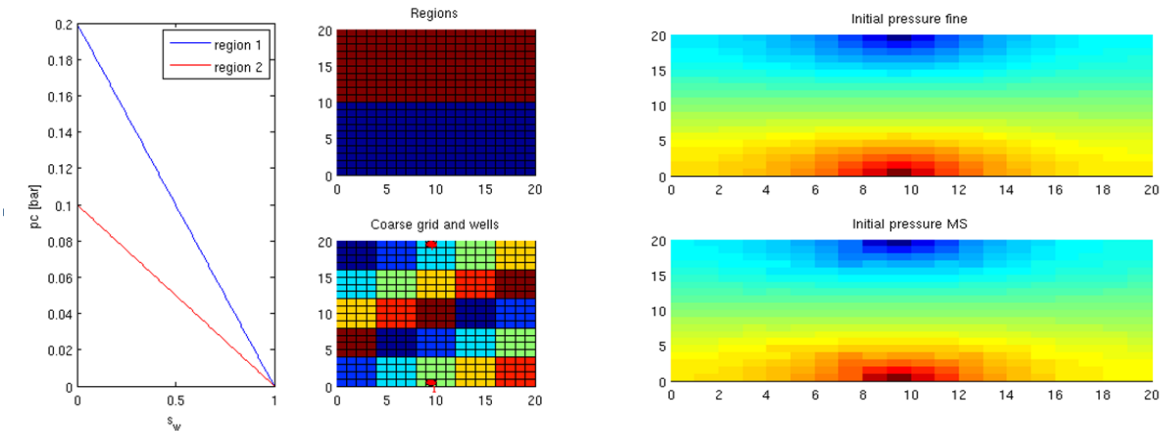

Figure 2 *The plots to the left show two different linear p_c curves corresponding to the two regions along, placement of injection and production well, and subdivision into coarse blocks. The plots to the right show the initial pressure distribution computed by the fine-scale and the multiscale solvers.*

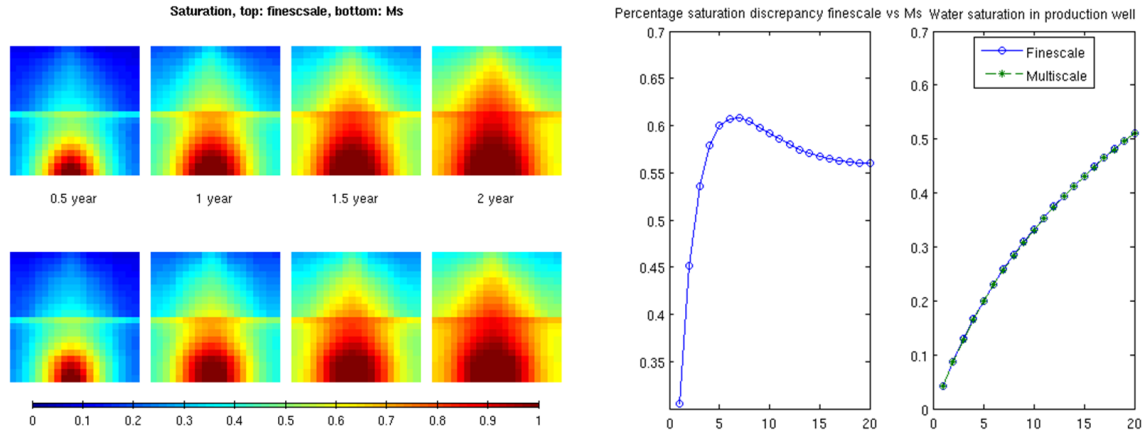

Figure 3 *The plots to the left show saturation profiles for the fine-scale and multiscale simulation for the box model. Capillary effects are clearly visible in the saturation distribution. The fine-scale and multiscale saturations are very similar. The plots to the right show the percentage discrepancy between fine-scale and multiscale simulation and water saturation in production well.*

from the bottom of the domain and oil is produced from the top. Gravity is acting in the z-direction. Transport loop runs with a pressure time step of 0.1 year. The initial fine-scale and multiscale pressure distribution are shown in Figure 2.

Figure 3 shows a comparison of the water saturation for the fine-scale and multiscale simulations. The capillary effects are visible in the plot with distinctly different behaviour of injected water in the upper and lower part of the domain. The multiscale simulation is able to capture the fine-scale effects nicely, giving an approximate solution that is only slightly different from the fine-scale solution. This is confirmed in the right part of the figure, which shows the percentage discrepancy between the fine-scale and the multiscale simulation along with curves depicting the corresponding saturations in the production well.

Example 2 (Sector model with nine regions) *Next, we consider a $21 \times 21 \times 13$ sector model that covers an area of 3×3 km^2 and has a thickness of approximately 100 m. The model has nine different saturation regions, shown in Figure 4, that each corresponds to a rock-type that is represented by its own relative permeability and capillary curves, shown in Figure 4. The porosity and permeability dis-*

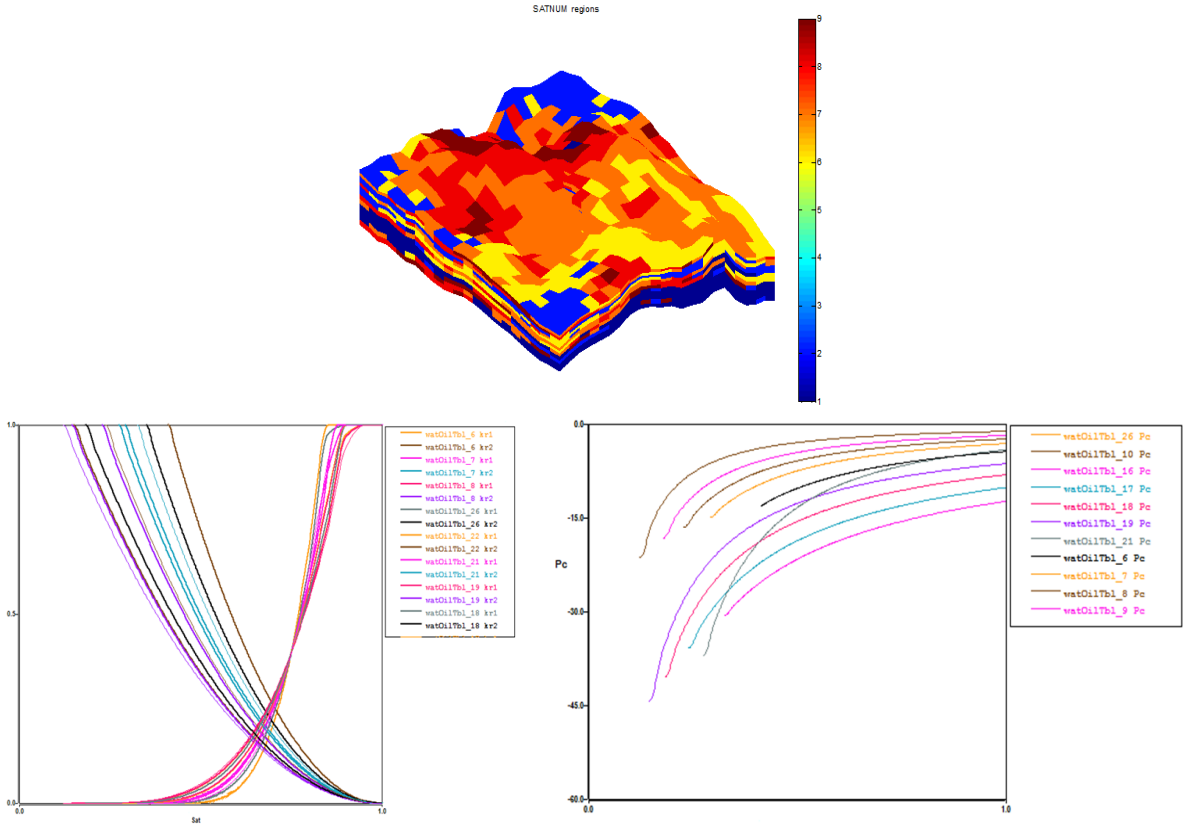

Figure 4 *The upper plot shows the sector model of a reservoir with nine different saturation regions. The lower plots show the corresponding relative permeability and capillary pressure curves.*

tributions are shown in Figure 5. The porosity values span the interval $[0.02, 0.12]$. *Similarly, the permeability varies from a minimum of 50 mD to a maximum of 400 mD in the model. The fine grid is partitioned into a* $5 \times 5 \times 3$ *coarse grid, as shown in Figure 5. The figure also shows the injector and producer, which are located at diagonally opposite corners of the model in a quarter of a 5-spot pattern. Initial reservoir pressure is 4728.23 psi. The injection well operates at a rate constraint of 3000 STB per day. The production well operates at a bottom-hole pressure constraint of 100 psi.*

Figure 6 shows the initial water saturation and the water saturation after twenty years computed by the fine-scale and the multiscale solvers. The two initial distributions are identical in the eye norm and clearly show the effect of different capillary and relative permeability curves in the different regions of the model. The saturation distributions after twenty years are not identical, but show the same qualitative

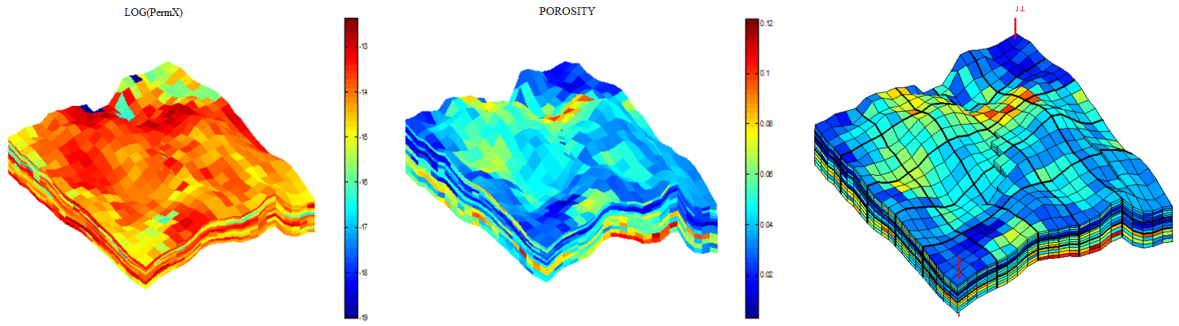

Figure 5 *The plots show the logarithm of the permeability (left), the porosity (middle), and the coarse grid (thick black lines) overlying the fine grid (thin black lines) and the placement of wells (right).*

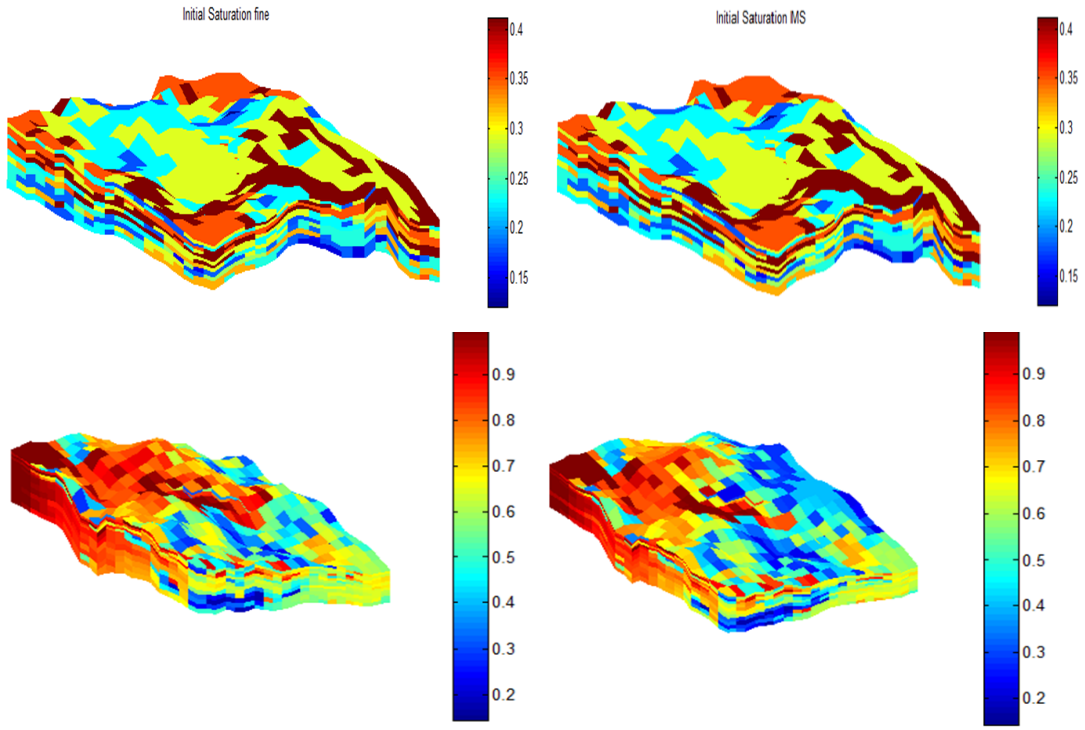

Figure 6 *Initial fine-scale and multiscale water saturation distribution. The saturation distribution clearly shows the effect of different capillary and relative permeability curves in different regions of the model. It can be seen that both models have similar initial water saturation*

behaviour. Figure 7 shows how the discrepancy between the two saturation distributions increases up to 4.25% until water breakthrough, but then starts to drop. Likewise, the saturation in the production well and the oil and water cut show that the breakthrough deviates slightly in the two simulations, but eventually the solutions seem to converge. Alltogether, the plots show that the multiscale simulation is able to account for gravity and spatial variations in capillary and relative permeability to capture reasonably accurate fine-scale details.

In the last test, we consider a compressible three-phase problem described by the black-oil equations. There are several ways to discretize and solve these equations, and a prerequisite for successful application of the MsMFE methodology is to have a robust numerical formulation for the fine-scale problem that solves the flow and transport in separate steps. To what extent such a formulation is available, is a question with a complex answer. In the next example, we will use a sequential method with a standard mixed formulation for the pressure equation and an implicit transport solver with saturation as primary variable. We tacitly assume that this is a reasonable solution strategy for the fine-scale equations.

Example 3 (Compressible three-phase flow) *The last test case involves a* $500 \times 500 \times 15m$ *box with a 3D heterogeneous permeability distribution represented on a* $10 \times 10 \times 3$ *grid. The model is initially filled with oil at 200 bar. The driving force is pressure difference between two wells that are located in opposite corners of the model with pressure 300 and 200 bar, respectively. Gas is the injected fluid. Both fluids are assumed to be compressible, with a compressibility of* $5 \cdot 10^{-3}$ *bar for the oil and the gas following an ideal gas law. The fluids have linear relative permeabilities and a viscosity of 1 cP for the oil and 0.1 cP for the gas. The permeability and the well placement are shown in Figure 8.*

The main strength of a multiscale method is, typically, its ability to robustly predict global responses in the system rather than predicting a pointwise accurate fine-scale solution. As our global measure, we therefore consider the oil and gas rates in the injector and producer, as well as the gas cut in the

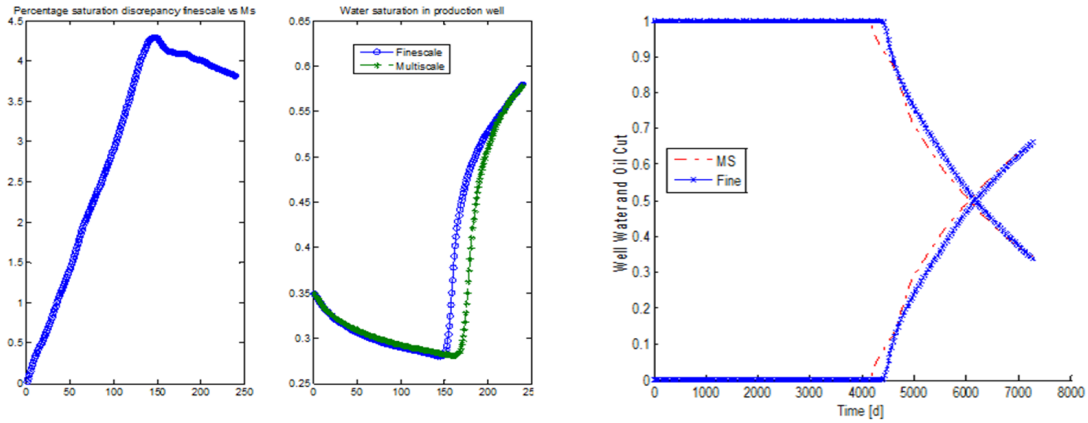

Figure 7 *The plots show, from left to right: percentage discrepancy between fine-scale and multiscale solution, water saturation in production well, and oil and water cut.*

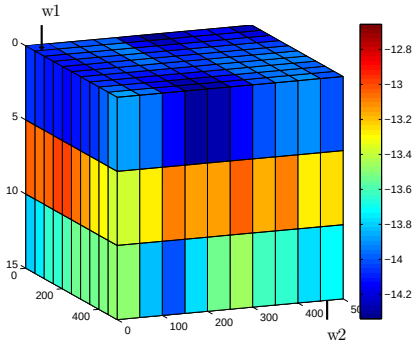

Figure 8 *Well placement and $\log_{10}$ of the permeability for the compressible three-phase test case.*

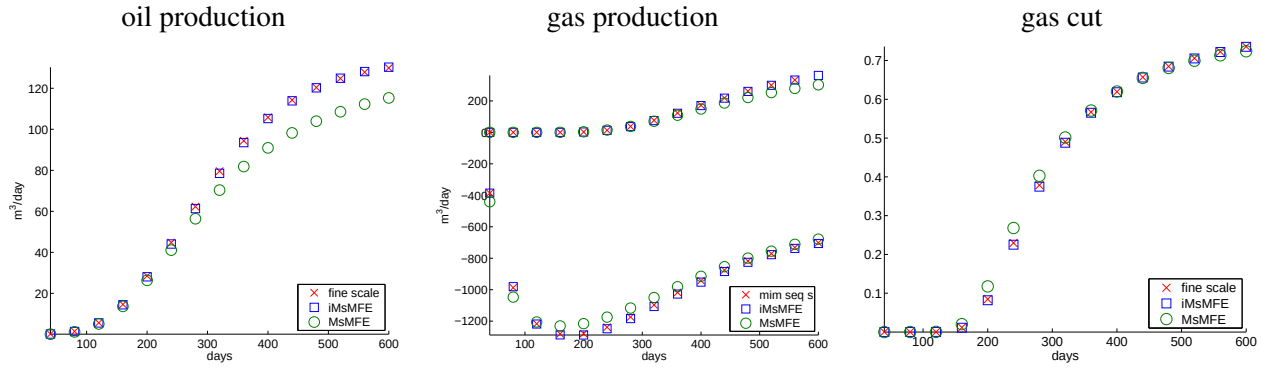

Figure 9 *Oil production, gas production, and gas cut computed by the fine-scale and the multiscale solvers for a 3D compressible three-phase test case.*

producer. These measures give all the information of the global response in our pressure-controlled systems. Figure 9 reports the results of the 3D simulation using a $5 \times 5 \times 1$ *coarse grid for the multiscale method. In the simulation, we used equally spaced time steps, each of length 40 days, to reach the final time of 600 days. From the results we can see that the oil production is underestimated by the MsMFE method, whereas the gas production and gas cut are calculated quite accurately. By adding extra iterations in the iMsMFE method, the multiscale method calculates a correct profile also for the oil production.*

Conclusions

In this paper we have reviewed a multiscale mixed finite-element method for incompressible two-phase flow and discussed how to the effects of capillary pressure. We report the result of two out of large series of benchmark tests that have been run to validate the method on models with a high degree of realism, including spatially dependent relative permeability and capillary effects, gravity, and highly heterogeneous rock properties specified on representative corner-point grids. Altogether, these benchmark cases show that the MsMFE method is efficient, robust and reasonably accurate, compared to the fine-scale simulation and hence has a significant potential for accelerating simulation of two-phase flow applications, particularly for incompressible flow. Compared with coarse-scale models, the accuracy and resolution of the fine-scale flux, pressure and saturation fields computed by the multiscale simulation are noteworthy. Combined with a large degree of robustness, this emphasizes the importance of the MsMFE method for its ability to capture fine-scale heterogeneity.

The MsMFE method can also be extended to compressible flow and has a certain potential both for weakly and strongly compressible problems, including black-oil methods. Here, however, the formulation of the method hinges on an effective operator-splitting method for the underlying fine-scale problem. Although good results can be obtained in many cases, there is a need for more research to improve the robustness of the methods for application to practical simulation of black-oil models of industry-standard complexity.

Acknowledgements

The authors would like to thank the Carbonate Research Team, Shell International Exploration and Production B.V., Rijswijk, The Netherlands for allowing us to publish this work.

References

[1] Aarnes, J.E. [2004] On the use of a mixed multiscale finite element method for greater flexibility and increased speed or improved accuracy in reservoir simulation. *Multiscale Model. Simul.*, **2**(3), 421–439 (electronic), ISSN 1540-3459.

[2] Aarnes, J.E. and Efendiev, Y. [2008] A multiscale method for modeling transport in porous media on unstructured corner-point grids. *J. Algorithms Comput. Technol.*, **2**(2), 299–318, doi: 10.1260/174830108784646616.

[3] Aarnes, J.E., Krogstad, S. and Lie, K.A. [2008] Multiscale mixed/mimetic methods on corner-point grids. *Comput. Geosci.*, **12**(3), 297–315, ISSN 1420-0597, doi:10.1007/s10596-007-9072-8.

[4] Alpak, F.O., Pal, M. and Lie, K.A. [2011] A multiscale method for modeling flow in stratigraphically complex reservoirs. *SPE Reservoir Simulation Symposium, The Woodlands, TX, USA, 21–23 February 2011*, doi:10.2118/140403-MS.

[5] Arbogast, T. [2002] Implementation of a locally conservative numerical subgrid upscaling scheme for two-phase Darcy flow. *Comput. Geosci.*, **6**(3-4), 453–481, ISSN 1420-0597.

[6] Arbogast, T. and Bryant, S.L. [2002] A two-scale numerical subgrid technique for waterflood simulations. *SPE J.*, **7**(4), 446–457.

[7] Audigane, P. and Blunt, M.J. [2004] Dual mesh method for upscaling in waterflood simulation. *Transp. Porous Media*, **55**, 71–89, ISSN 0169-3913, 10.1023/B:TIPM.0000007309.48913.d2.

[8] Chen, A. and Hou, T. [2002] A mixed multiscale finite element method for elliptic problems with oscillating coefficients. *Math. Comp.*, **72**(242), 541–576.

[9] Chen, Y. and Durlofsky, L.J. [2006] Adaptive local-global upscaling for general flow scenarios in heterogeneous formations. *Transp. Porous Media*, **62**(2), 157–182.

[10] Chen, Y., Durlofsky, L.J., Gerritsen, M. and Wen, X.H. [2003] A coupled local-global upscaling approach for simulating flow in highly heterogeneous formations. *Adv. Water Resour.*, **26**(10), 1041–1060.

[11] Efendiev, Y. and Hou, T.Y. [2009] *Multiscale Finite Element Methods*, vol. 4 of *Surveys and Tutorials in the Applied Mathematical Sciences*. Springer Verlag.
[12] Farmer, C.L. [2002] Upscaling: a review. *Int. J. Numer. Meth. Fluids*, **40**(1–2), 63–78, doi:10.1002/fld.267.
[13] Guerillot, D. and Verdiere, S. [1995] Different pressure grids for reservoir simulation in heterogeneous reservoirs. *SPE Reservoir Simulation Symposium, 12-15 February 1995, San Antonio, Texas, USA*, doi:10.2118/29148-MS.
[14] Hajibeygi, H. and Jenny, P. [2009] Multiscale finite-volume method for parabolic problems arising from compressible multiphase flow in porous media. *J. Comput. Phys*, **228**(14), 5129 – 5147, ISSN 0021-9991, doi:10.1016/j.jcp.2009.04.017.
[15] Hajibeygi, H. and Jenny, P. [2011] Adaptive iterative multiscale finite volume method. *J. Comput. Phys*, **230**(3), 628 – 643, ISSN 0021-9991, doi:10.1016/j.jcp.2010.10.009.
[16] Hou, T.Y. and Wu, X.H. [1997] A multiscale finite element method for elliptic problems in composite materials and porous media. *J. Comput. Phys.*, **134**(1), 169–189.
[17] Jenny, P., Lee, S.H. and Tchelepi, H.A. [2003] Multi-scale finite-volume method for elliptic problems in subsurface flow simulation. *J. Comput. Phys.*, **187**, 47–67.
[18] Kippe, V., Aarnes, J.E. and Lie, K.A. [2008] A comparison of multiscale methods for elliptic problems in porous media flow. *Comput. Geosci.*, **12**(3), 377–398, ISSN 1420-0597, doi:10.1007/s10596-007-9074-6.
[19] Krogstad, S. and Lie, K.A. [2012] Multiscale mixed finite-element methods for compressible flow.
[20] Krogstad, S., Lie, K.A., Nilsen, H.M., Natvig, J.R., Skaflestad, B. and Aarnes, J.E. [2009] A multiscale mixed finite-element solver for three-phase black-oil flow. *SPE Reservoir Simulation Symposium, The Woodlands, TX, USA, 2–4 February 2009*, doi:10.2118/118993-MS.
[21] Lamine, S. and Edwards, M.G. [2009] Higher order multidimensional wave oriented upwind schemes for flow in porous media on unstructured grids. *SPE Reservoir Simulation Symposium, The Woodlands, TX, USA, 2–4 February 2009*, doi:10.2118/119187-MS.
[22] Lamine, S. and Edwards, M.G. [2010] Higher order multidimensional upwind convection schemes for flow in porous media on structured and unstructured quadrilateral grids. *SIAM J. Sci. Comput.*, **32**(3), 1119–1139, ISSN 1064-8275, doi:10.1137/080727750.
[23] Lee, S.H., Wolfsteiner, C. and Tchelepi, H. [2008] Multiscale finite-volume formulation for multiphase flow in porous media: Black oil formulation of compressible, three phase flow with gravity. *Comput. Geosci.*, **12**(3), 351–366, doi:10.1007/s10596-007-9069-3.
[24] Lie, K., Krogstad, S., Ligaarden, I., Natvig, J., Nilsen, H. and Skaflestad, B. [2012] Open-source MATLAB implementation of consistent discretisations on complex grids. *Comput. Geosci.*, **16**, 297–322, ISSN 1420-0597, 10.1007/s10596-011-9244-4.
[25] Pal, M. and Edwards, M.G. [2007] Quasimonotonic continuous darcy-flux approximation for general 3d grids of any element type. *SPE Reservoir Simulation Symposium, The Woodlands, TX, USA, 26–28 February 2007*, doi:10.2118/106486-MS.
[26] Pal, M., Edwards, M.G. and Lamb, A.R. [2006] Convergence study of a family of flux-continuous, finite-volume schemes for the general tensor pressure equation. *Internat. J. Numer. Methods Fluids*, **51**(9-10), 1177–1203, ISSN 0271-2091, doi:10.1002/fld.1211.
[27] SINTEF [2011] Matlab Reservoir Simulation Toolbox (MRST), version 2011a. `http://www.sintef.no/MRST`.
[28] Wheeler, M.F., Xue, G. and Yotov, I. [2012] A multiscale mortar multipoint flux mixed finite element method. *ESAIM*, **46**(4), 759–796, ISSN 0271-2091.